Progress In Electromagnetics Research C, Vol. 138, 65–78, 2023

A Novel Square Array Reflector Plate Equipped Mushroom Cloud Patch Antenna

Maniram Ahirwar* **and Virendra S. Chaudhary**

Abstract—A Mushroom-Cloud-shaped wide slot microstrip patch antenna (MC-MSPA) was discovered and proved to be a viable option for wideband applications in this research study. The given antenna has a high radiation and wideband reflection coefficient of 134.47% from 1.15 GigaHz to 5.87 GigaHz for $|S_{11}| < -10$ dB. This antenna has a peak gain of 6.47 dBi at 4.6 GigaHz and 6.1 dBi at 5 GigaHz, as well as an return loss of 47.37 dB at 1.88 GHz. MC-MSPA has optimised dimensions of $0.73\lambda_g \times 0.72\lambda_g \times 0.02\lambda_g$. Furthermore, a reflecting surface of a 7×7 square-shaped array beneath the ground plane has been included to provide even higher gain and directivity. The proposed MC-MSPA+RP antenna has a fractional bandwidth of 63% with dual bands from 1.438 to 2.782 GigaHz and 38.89% from 3.964 to 5.878 GigaHz, with a peak gain of 9.657 dBi, maximum directivity of 10.44 dBi at 5 GigaHz, and maximum return loss of 54 dB at 4.9 GigaHz. Reflector plate electrical dimensions have been enhanced to $0.87\lambda_g \times 0.87\lambda_g \times 0.24\lambda_g$. The proposed design improves gain and directivity, both of which are important for WLAN and Wi-MAX applications.

1. INTRODUCTION

Modern wireless communication systems including military, mobile, aviation, and others employ microstrip patch antenna [1]. For high gain and long-targeted distance, remote sensing, radar, and satellite applications have employed antennas incorporating reflectors [2]. High gain, low profile, low voltage standing wave ratio (VSWR), low cross-polarization, budget cost, light weight, simple construction, and low-cost manufacturing are all benefits of these antennas [3]. Microstrip antennas have poor bandwidth, gain, and directivity [4]. Many research academics have been improving microstrip antenna gain and directivity utilizing various designs, concepts, and materials. Different methods are employed to attain suitable antenna performance characteristics, including reflecting surface [5–7], array element [8], fractal boundary [10, 11], and metasurface material antenna [9, 13], along with unique arbitrary shapes inspired by nature like flower [12]. Al-Gburi et al. [14], thorough research employed a printed monopole antenna with a strawberry-shaped radiating patch on an FR-4 dielectric substrate with a coplanar waveguide and frequency selective surface (FSS) to obtain high bandwidth and gain. In this study, an antenna with single-layer reflector showed excellent agreement in gain maintained between 7.87 dBi and 9.68 dBi and steady radiation pattern for ground-penetrating radar (GPR). By adding a magnetic conductor and a multi-band antenna, Gan et al. [15] increased the antenna's performance. By varying the slot length on the metal plate with the defective ground structure, the developed antenna's performance has been improved. The bands are ideal for WLAN and Wi-MAX services. At 7.9 GHz, the antenna's max gain is 8.6 dBi. For wearable applications, Yuan et al. [17] suggested a flexible substrate antenna with a hexagon unit reflector. Artificial magnetic conductor (AMC) reflectors were employed to improve the antenna's reflection coefficient ($|S_{11}|$) at 2.4 GHz, directional radiation pattern, and gain to 6.68 dBi [19] suggested by Kundu et al. A reflective plate was made of two layers of frequency selective

Received 20 August 2023, Accepted 17 September 2023, Scheduled 2 October 2023
* Corresponding author: Maniram Ahirwar (maniram.ahirwar@mp.gov.in).
The authors are with the Department of Electronics and Communication Engineering, RKDF University, Gandhinagar, Bhopal, India.

surface (FSS) with a 4×4 array. Gain and impedance bandwidth are improved by optimising antenna-reflector plate space. Metamaterial was employed to unite FSS layers. 8.5 dBi peak gain is attained. Back to Portable (B.T.P.) can use ground-penetrating radar on this. The circular monopole antenna with coplanar waveguide feed shown in [23] is $64 \times 56 \times 18.2\,\text{mm}^3$ on FR-4 material. The antenna's gain was increased by using a mushroom-shaped FSS as a reflecting device. Operating dual bands are from 3.5 to 4.5 GHz and 7.5 to 8 GHz of frequency. The highest directivity is 3.4 dB, and the peak gain is 7 dBi. A partially reflective surface EBG resonator mentioned in [24] has an impressively slim profile at just 1.6 mm thickness while delivering an effective bandwidth of 12.6%. Its measured peak gain reaches an impressive 16.2 dBi at 11.5 GHz, and it maintains a 3 dB gain bandwidth of 15.7%.

This inquiry planned, analyzed, studied, and produced the mushroom cloud-shaped microstrip patch antenna (MC-MSPA), which had a wide fractional bandwidth of 137.97% from 1.126 GHz to 6.136 GHz $|S_{11}| < -10$ dB. The high gain MC-MSPA loaded with a square reflector plate antenna (MC-MSPA+RP) has been created for Wi-MAX and WLAN applications to improve antenna gain and directivity. A dual-band bi-directional radiation pattern with peak gain of 9.657 dBi and maximum directivity of 10.34 dBi at 5 GHz is offered by the suggested antenna.

2. ANTENNA CONFIGURATION

Figure 1 shows the two-dimensional characteristics of the proposed MC-MSPA on the $z = 0$ axis with 0.035 mm thick copper-simulated conductive layers. With L&W limitations, a 50-ohm ($F_w \times F_l$) feed

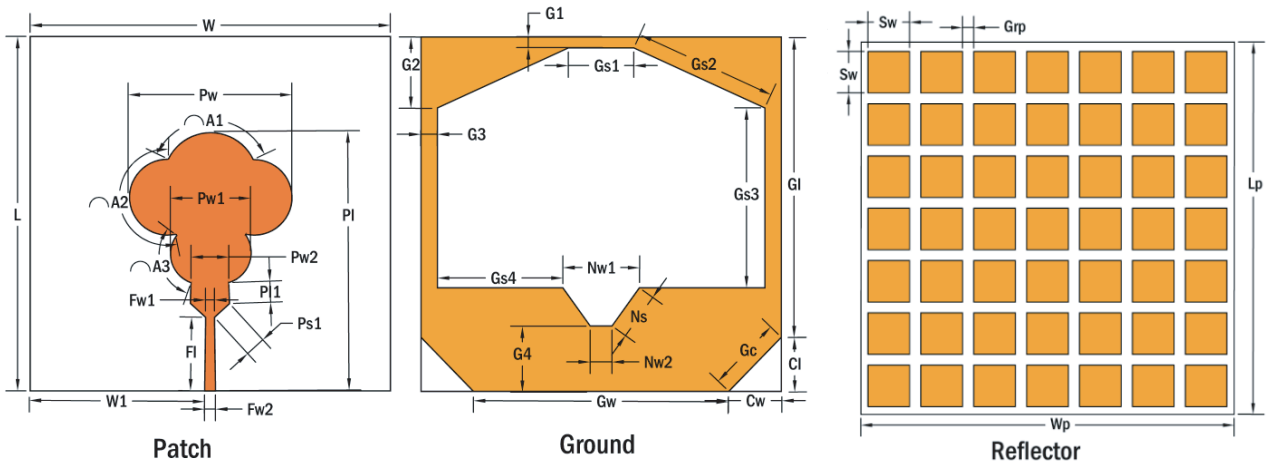

Figure 1. Design parameter of Mushroom Cloud-Shaped Microstrip Antenna.

Table 1. Optimized antenna design parameters (in mm).

Parameter	Value	Parameter	Value	Parameter	Value	Parameter	Value
W	66	F_L	13.5	G_1	2	Gs_2	26.4
L	65	F_{w1}	1.65	G_2	13	Gs_3	33
P_w	30	F_{w2}	2	G_4	12	Gs_4	23
P_L	47.55	P_{w1}	14.67	G_w	46.77	A_1	19.43
P_{l1}	3.85	P_{w2}	6.91	G_c	13.82	A_2	23.44
P_{s1}	3.74	G_l	55	Gs_1	12	A_3	10.54
S_W	9	G_{rp}	2.1	W_P, L_P	72	T_A, T_P	1.6
N_{W1}	14	N_{w2}	4	N_S	8.6	C_L	10
C_W	9.6	G_h	17	G_3	2		

line was constructed on the top layer of an FR-4 substrate ($\tan(\delta) = 0.02$, $r = 4.3$, and $h = 1.6\,\text{mm}$). The substrate's back and the mushroom cloud-shaped tuning element's A_1, A_2, and A_3 parameters terminate it. The ground plane has a triangular notch and a wide slit. The aerial's radiating patch and ground plane interface are optimized. The ground plane corners feature parasitic triangle-shaped slots. In Figure 3, the mushroom-cloud shaped microstrip antenna loaded with a 7×7 square-shaped reflector (MC-MSPA+RP) is placed below the ground plane at $z = -26.635$ plane with an air gap of 17 mm, copper layer width of 0.035 mm, and FR-4 substrate width of 1.6 mm to improve gain and directivity. Parametric studies optimised the MC-MSPA and MC-MSPA+RP antenna dimensions in Table 1 in mm.

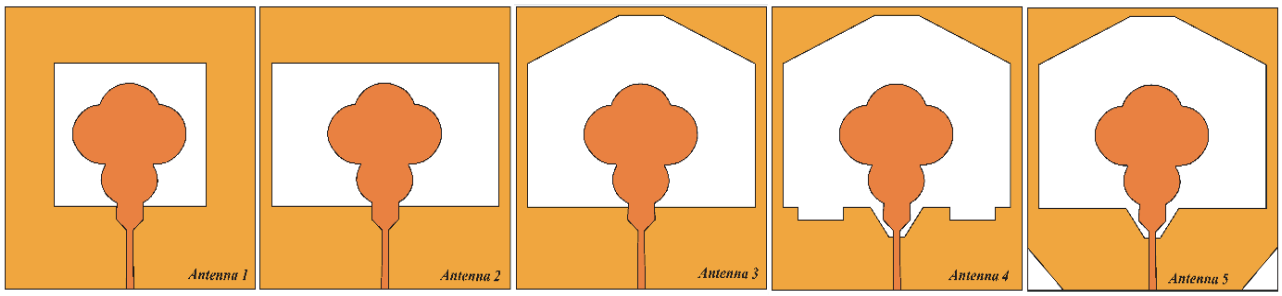

Figure 2. Evolution of mushroom-cloud shaped microstrip patch antenna (MC-MSPA).

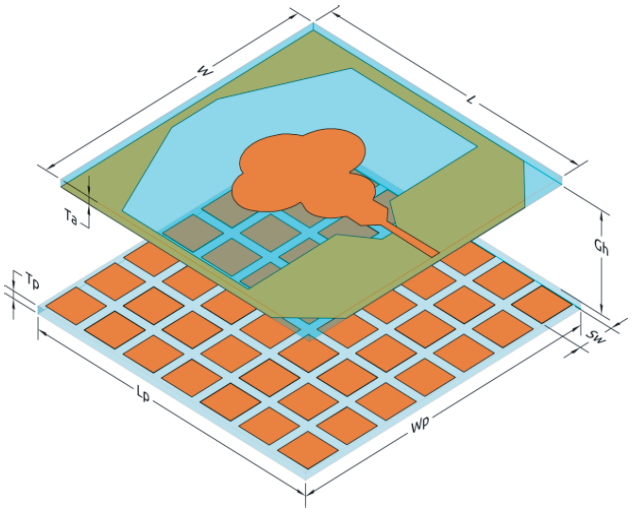

Figure 3. 3D view of square reflector mushroom-cloud shaped microstrip patch antenna (MC-MSPA).

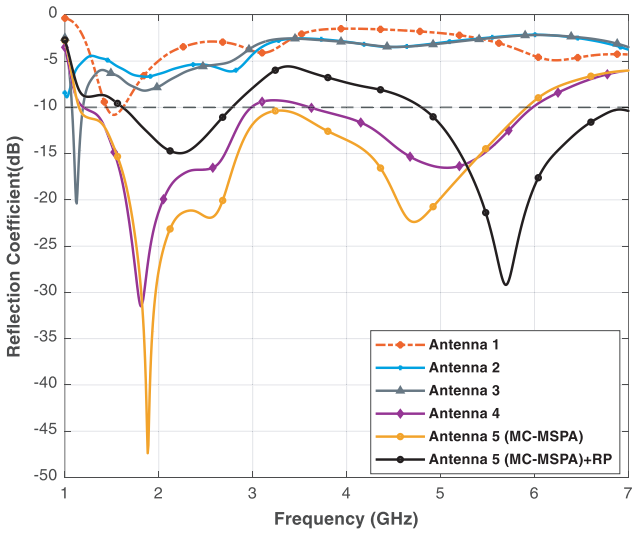

Figure 4. Analyses of the reflection coefficient's ($|S_{11}|$) performance of Antenna 1, 2, 3, 4, 5 & 5 + Reflector.

3. EVOLUTION OF ANTENNA

Figure 2 depicts MC-MSPA evolution. The next five processes optimize the ground plane to maximize antenna performance. Antenna 1 features a rectangular huge slot-shaped notch. Antenna 2 has a taller rectangular slot.

Further in Antenna 3, the notch has been cut in the center beneath the microstrip feed line. In Antenna 4, two curves have been incorporated on the ground plane. In the final stage in Antenna 5, two triangle-shaped parasitic slots have been incorporated at the corners of the ground plane. In Figure 4, reflection coefficient ($|S_{11}|$) performance evaluation of antennas 1, 2, 3, 4, & 5, and it is found that Antenna 5 has reached its optimum level and found broad impedance bandwidth characteristics.

Antenna 1 does not reveal more extended impedance bandwidth except for a −10 dB slight dip at 1.5 GHz frequency, referring to Equation (2) for the formula. Antenna 2 does not exhibit any reflection coefficient −10 dB characteristics. Antenna 3 has a slight dip of reflection coefficient with minimum $|S_{11}|$ of −20.1 dB from 1 GHz to 1.23 GHz. Antenna 4 has a dual-band reflection coefficient characteristic which has been found from 1.23 to 3 GHz and from 3.5 GHz to 6 GHz, but the wideband impedance characteristics are required; therefore, Antenna 5 exhibits a wideband impedance bandwidth of 134.47% from 1.15 GHz to 5.87 GHz for $|S_{11}| < -10$ dB.

4. PARAMETRIC STUDY

The antenna structure was analysed using a parametric sweep. The antenna's gain, directivity, and return loss are optimised. The antenna's gain, directivity, and frequency response are affected by parameters S_w, F_w, G_3, N_{w1}, and G_h. To optimise the proposed antenna's performance, these factors are crucial. To assess antenna performance, one parameter is modified.

4.1. Impact of Square Element Width (S_w) on Reflection Coefficient (S_{11})

Figure 5 shows the antenna's performance after adjusting the square element width (S_w) and shows the return loss characteristics during changing the reflecting plate's square width, which was recorded. The square's width is 7–11 mm. For square widths above 9 mm, the antenna has a single band. The effective dual-band return loss characteristics were attained at $S_w = 7$ mm by lowering S_w. Thus, the antenna's 7 mm breadth may improve return loss but not gain performance.

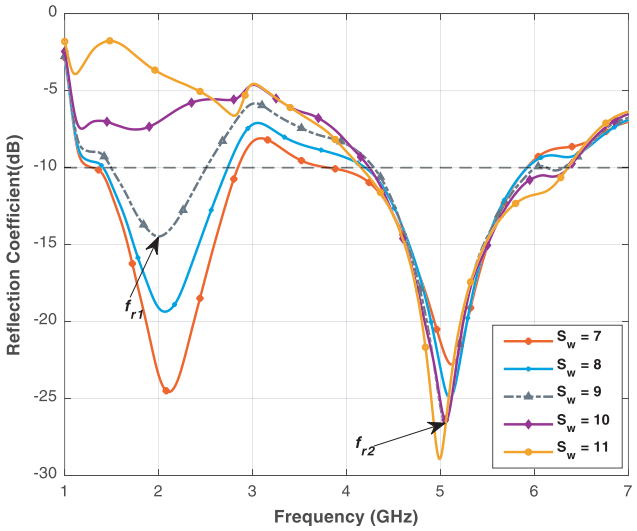

Figure 5. Simulated reflection characteristics for distinct values of square element width.

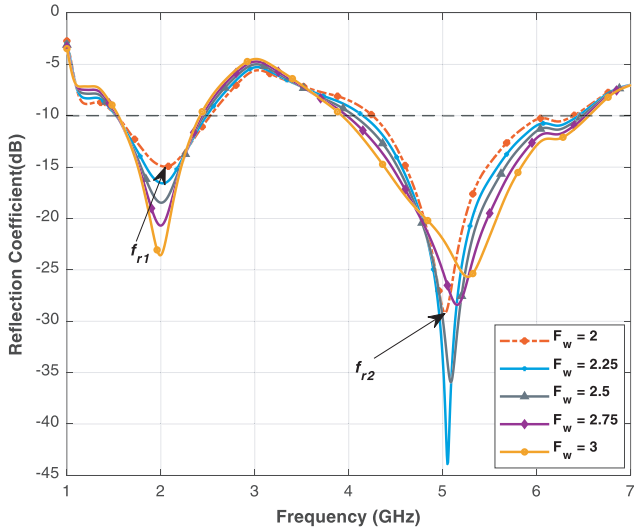

Figure 6. Simulated reflection characteristics for distinct values of Feed Line Width.

4.2. Changes in Reflection Coefficient ($|S_{11}|$) as a Function of Feedline Width (F_w)

From 2 mm to 3 mm, feedline width (F_w) was studied for antenna performance. The lower value of F_w converts antenna characteristics from dual bands to single band. Figure 6 demonstrates that the second band needs a minimum F_w value of 2 mm while the first band needs a maximum of 3 mm. The two bands agree at $F_w = 2.5$ mm, hence feed width must be limited for excellent return loss. The resonance frequency f_{r2} is changed by 0.01 GHz in the lower band from $F_w = 2.5$ mm to 5.413 GHz.

4.3. Impact of Side Width of the Ground Plane (G_3) on Reflection Coefficient ($|S_{11}|$)

The side width of the ground plane (G_3) affects the planned antenna's simulated return loss characteristics ($|S_{11}|$) (refer to Figure 7). G_3 substantially impacts the antenna band's bandwidth, because it greatly impacts the mutual coupling between the radiating patch and the antenna's ground plane. G_3 ranged from 2 to 6 mm. Both bands have a reasonable bandwidth for $G_3 = 2$ mm; however at $G_3 > 2$ mm, their bandwidth starts to decrease, which is caused by ground-patch electromagnetic coupling. G_3 shifts f_{r2} from 4.8 GHz to 5.1 GHz but does not shift f_{r1}.

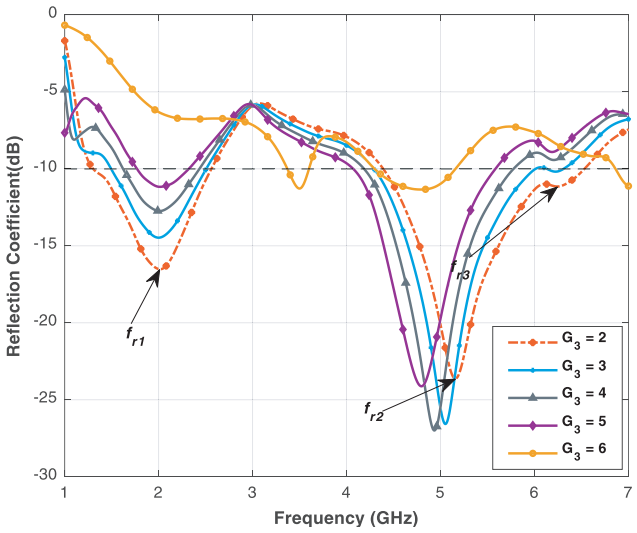

Figure 7. Simulated reflection characteristics for distinct values of side width of the ground plane.

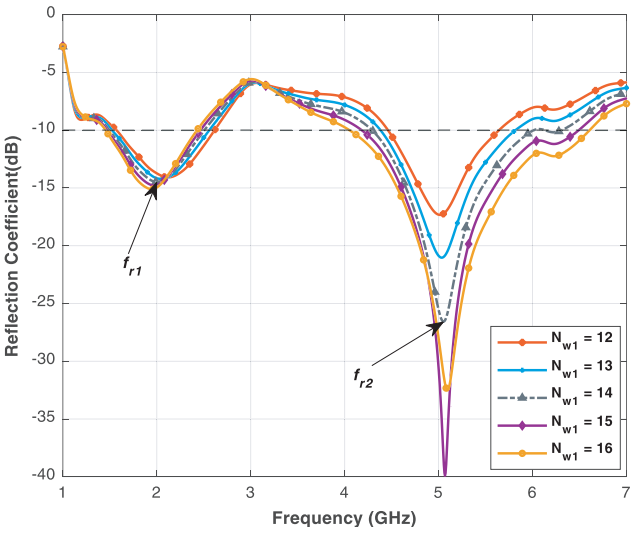

Figure 8. Simulated reflection characteristics for distinct values of top-notch width.

4.4. Impact of Top-Notchwidth (N_{w1}) on Reflection Coefficient ($|S_{11}|$)

As indicated in Figure 8, N_{w1}'s top-notch width ranges from 12 to 16 mm. The lower resonance frequency f_{r1} has been adjusted from 2.1 GHz to 1.9 GHz; however, the higher resonance frequency f_{r2} has changed little in the upper band. The higher band's impedance bandwidth was more affected by N_{w1} than the lower band. Reflection is good for $N_{w1} = 16$.

4.5. Impact of the Gap between Antenna and Reflection Plate (G_h) on Gain

The gap between antenna and reflecting plate (G_h) indicated in Figure 9 has been changed from 13 mm to 21 mm to obtain the suggested antenna's high gain performance. $G_h = 17$ mm yielded a peak gain of 9.332 dBi at 5 GHz. Placing the reflector below the ground at an adequate spacing exploits undesirable back radiation and stimulates the radiation upward, resulting in acceptable antenna performance characteristics.

4.6. Impact of the Gap between Antenna and Reflection Plate (G_h) on Directivity

In order to obtain high directivity performance of the proposed antenna, the gap between antenna and reflection plate (G_h) has been varied from 13 mm to 21 mm, and maximum directivity of 10 dBi is found at frequencies 5 GHz, 5.5 GHz, and 6.5 GHz for $G_h = 15$ mm, 13 mm, and 19 mm, respectively, as shown in Figure 10. However, the bad effect on another impedance bandwidth parameter and the modest value of $G_h = 17$ produce the best correlation between gain and impedance bandwidth parameters.

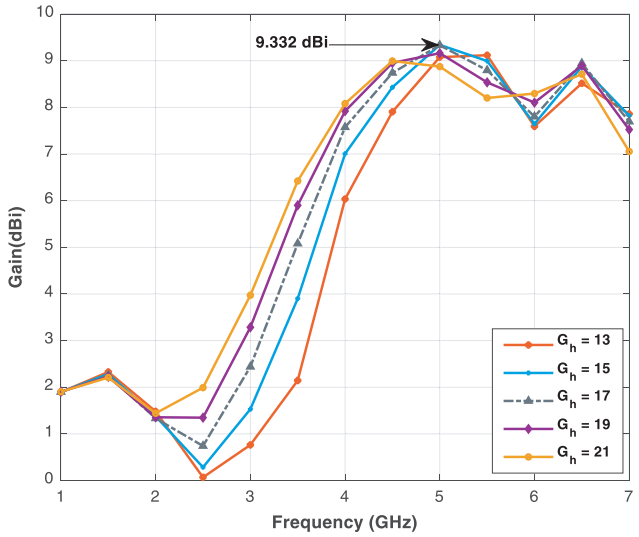

Figure 9. Simulated peak gain of the antenna for distinct values of gap (G_h).

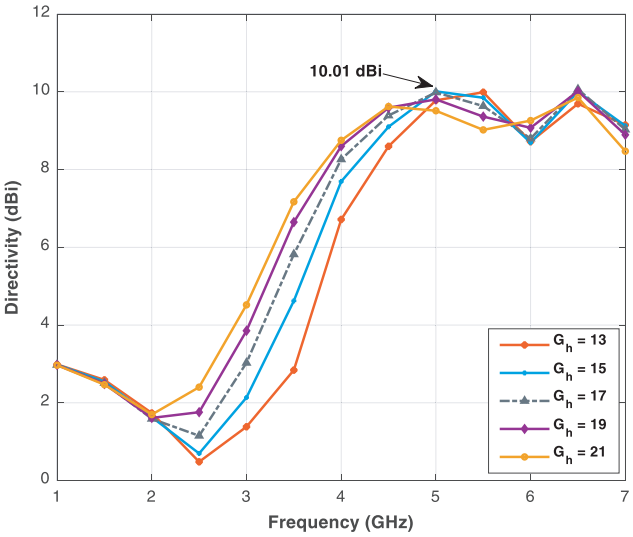

Figure 10. Simulated directivity of antenna for distinct values of gap (G_h).

4.7. Impact of the Square Size of Reflector Plate (S_w) on Gain

Figure 11 shows how the reflector plate's square size (S_w) affects antenna gain. This value affects gain performance because the reflector has both capacitive (line spacing between squares) and inductive (square-shaped grid) qualities. The maximum gain value is above 10 dB for $S_w = 10$ mm and higher. At 4.5 GHz and 6 GHz, $S_w = 11$ mm yielded maximum gain values above 10 dBi. However, another impedance bandwidth parameter showed a negative influence. Thus, $S_w = 9$ mm provides the best connection between gain and impedance bandwidth characteristics.

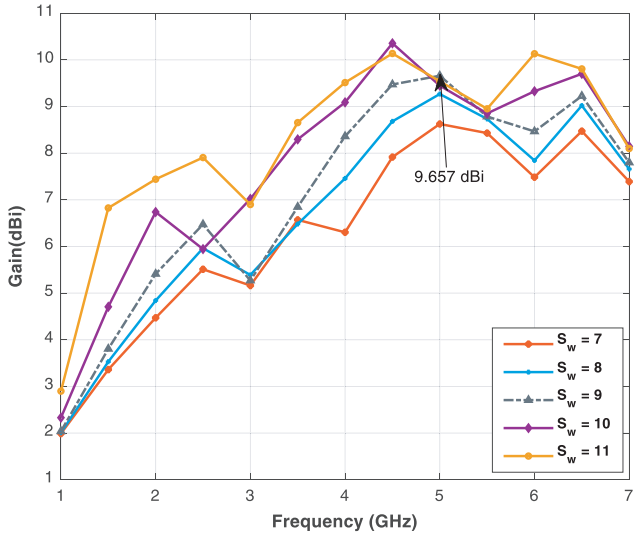

Figure 11. Simulated peak gain of the antenna for distinct values of square width of the reflector plate.

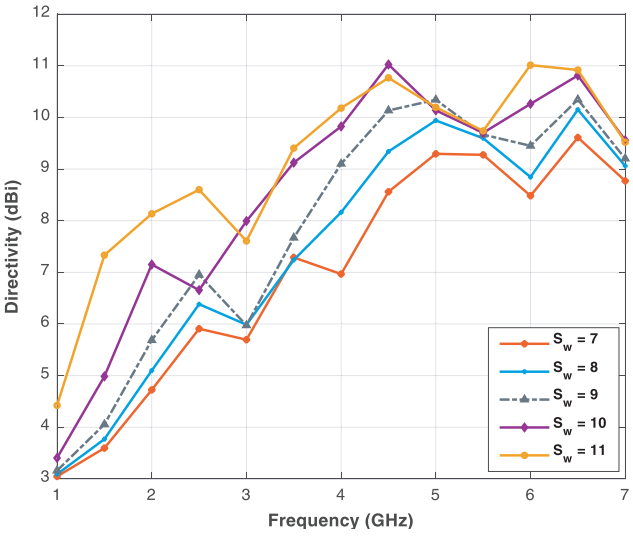

Figure 12. Simulated directivity of antenna for distinct values of square width of the reflector plate.

4.8. Impact of Square Width (S_w) on Directivity of the Antenna

The impact of the square size of the reflector plate (S_w) on the directivity of the antenna is shown in Figure 12. For the value of $S_w = 10$ mm and 11 mm, the value of maximum directivity has reached up to 11 dBi at 4.5 GHz and 6 GHz, respectively. However, the adverse effect was found on another impedance bandwidth parameter. Accordingly, the moderate value of $S_w = 9$ mm gives the batter correlation among directivity, gain, and impedance bandwidth parameters, which is preferable to any other values of S_w.

5. EXPERIMENTAL ANALYSIS

The fabricated mushroom cloud-shaped wide slot microstrip patch antenna is depicted in Figure 13, and Figure 14 shows the fabricated MC-MSPA loaded with 7×7 square array reflector.

Computer Simulation Technology (CST) Microwave optimised the antenna and results. Network Analyzer provided experimental results. Figure 15 shows simulated versus measured return loss ($|S_{11}|$) frequency characteristics. The antenna has 137.97% fractional bandwidth from 1.126 GHz to 6.136 GHz for $|S_{11}| < -10$ dB. This antenna has a peak gain of 6.29 dBi at 4.7 GHz, 6.1 at 5 GHz, and -47.37 at

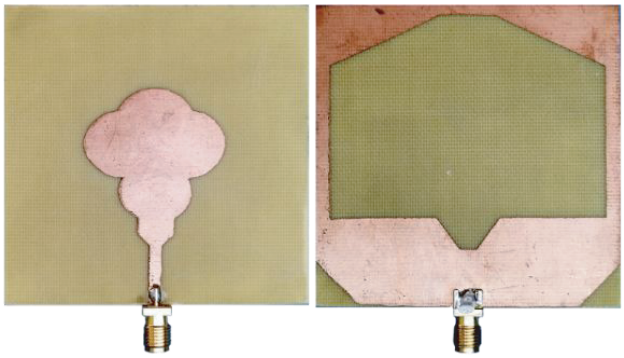

Figure 13. Fabricated design of MC-MSPA.

Figure 14. MC-MSPA+RP (3D-view).

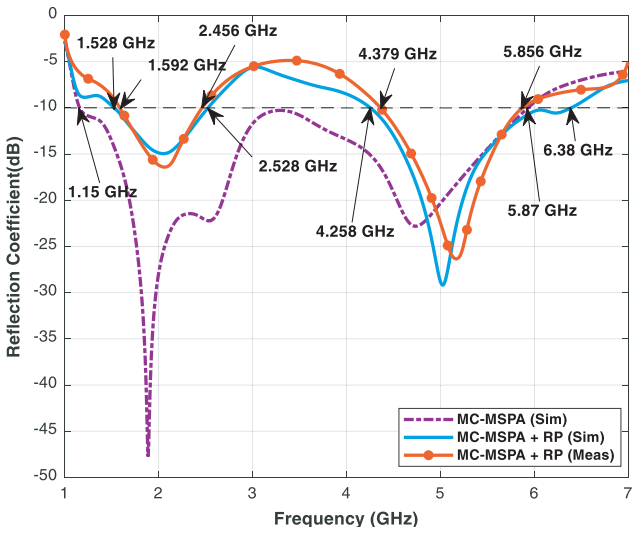

Figure 15. Return loss comparison with cut-off frequencies.

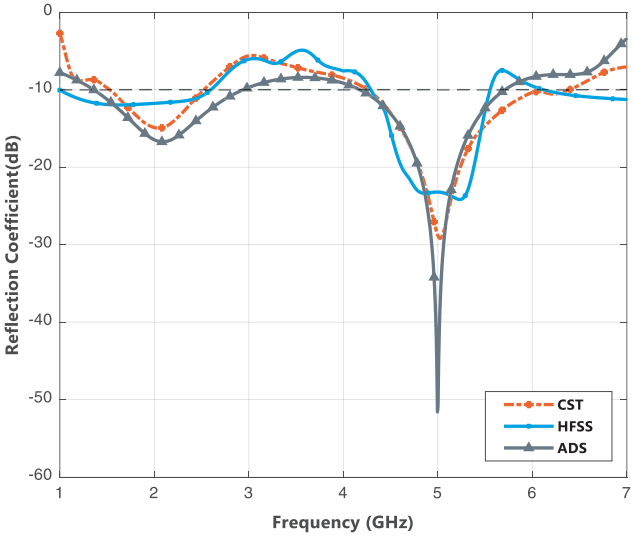

Figure 16. Return loss characteristics comparison of CST, HFSS, and ADS.

1.88 GHz. MC-MSPA's optimised electrical dimensions are 66 mm × 65 mm × 1.6 mm.

MC-MSPA+RP's square-shaped reflecting surface below 17 mm boosts gain and directivity. MC-MSPA+RP has 63% fractional bandwidth from 1.438 to 2.782 GHz and 38.89% from 3.964 to 5.878. Figure 15 compares MC-MSPA+RP reflection coefficient $|S_{11}|$.

Measured results are similar to simulation ones. Feed probe disruption, permittivity problems, fabrication variations, and measuring circumstances might cause errors. Figure 16 shows CST, High Frequency Structure Simulator (HFSS), and Advanced Design System (ADS) MC-MSPA+RP simulations.

5.1. Simulated and Measured Results

5.1.1. Simulated Bandwidth of MC-MSPA

The calculated bandwidth of the designed antenna is 134.47% over the range of 1.15 to 5.87 Ghertz using Equation (1).

$$Fractional\ Bandwidth\ (FBW) = 200 \times \left(\frac{f_H - f_L}{f_H + f_L}\right)\% \tag{1}$$

$$Impedance\ Bandwidth\ (IBW) = f_H - f_L \tag{2}$$

5.1.2. Simulated Bandwidth of MC-MSPA with Reflector Plate

First Band — The calculated fractional bandwidth of the proposed antennas is 63% for the frequency range of 1.528–2.528 Ghertz.

Second Band — The calculated fractional bandwidth of the proposed antennas is 38.89% for the frequency range of 4.258–6.38 Ghertz.

5.1.3. Measured Bandwidth of MC-MSPA with Reflector Plate

First Band — From 1.592 to 2.456 Ghertz, the designed antenna has yielded a fractional bandwidth of 42.68 percent in measurements.

Second Band — Simulated findings show that the designed antenna has a fractional bandwidth of 28.86% in the frequency range of 4.379 to 5.856 GHertz.

A small error has occurred between measured and simulated bandwidths. It may be due to the fabrication precision of the antenna or losses of the measuring system.

5.2. Equivalent Circuit Model of MC-MSPA with Reflector

The equivalent circuit model of the MC-MSPA+RP is shown in Figure 17. The circuit consists of a combination of (L_1), capacitance (C_1), and resistance (R_1) in parallel and series (refer to Table 2). The equivalent circuit model designed by the ADS has five pairs of inductors and capacitors connected in parallel. Each pair is responsible for peaks and dips in the reflection characteristics of the antenna.

Table 2. Equivalent RLC circuit values from ADS.

Components	Values	Components	Values
C_1	0.022 fF	L_1	0.056 fH
C_2	0.430 pF	L_2	2.163 nH
C_3	1.189 aF	L_3	4.295 nH
C_4	0.280 pF	L_4	0.025 pH
C_5	0.3672 pF	L_5	4.756 nH
R_1	106.482 Ohms		

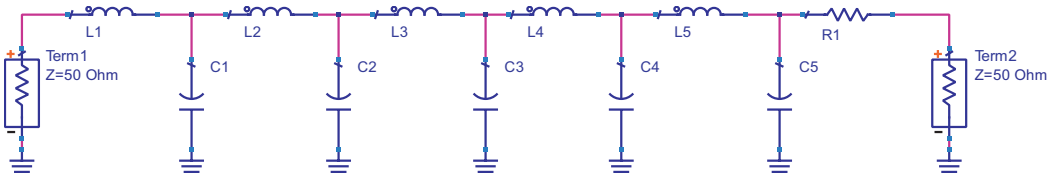

Figure 17. ADS RLC equivalent circuit of proposed reflector plate Mushroom Cloud-shaped wide slot MSPA using ADS.

5.3. Current Distribution

Current distributions of the proposed antenna at CST simulated resonating frequencies are shown in Figure 18. To verify the resonance 2.008 GHz frequency, current vectors go lower and peak at patch P1. At 4.93 GHz, current vectors move downhill through patch P2's edge at the microstrip feed point's linked patch element.

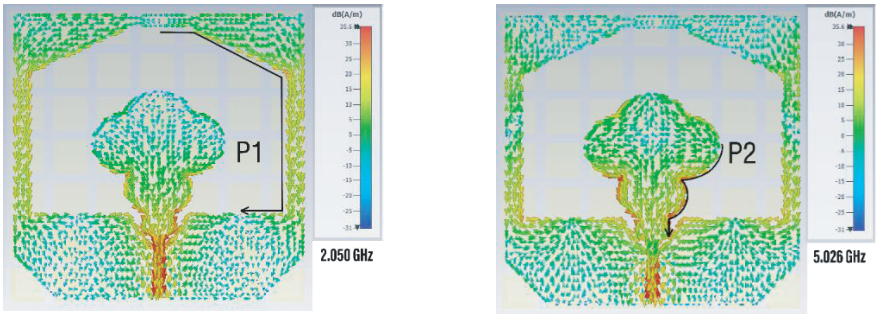

(a) (b)

Figure 18. Surface current distribution of proposed antenna, (a) 2.050 GHz, and (b) 5.026 GHz.

5.3.1. 1st Harmonic

The current vectors at the initial resonance frequency of 2.05 GHz flow clockwise from the top centre of the ground slot, down the inside edge of the slot, and into the bottom centre of the slot along the side (refer to Figure 18(a)). The 2.05 GHz frequency signals are the result of the radiations through this current path (P_1) as shown in Figure 18(a). The length of this route can be calculated with Equation (3).

$$P_1 = \frac{G_{s1}}{2} + G_{s2} + G_{s3} + \frac{G_{s4}}{2} \tag{3}$$

$$f_{r1} = \frac{c}{P_1\sqrt{\varepsilon_{eff}}} \tag{4}$$

The determined value of f_{r1} is 1.97 GHz, and the length of the present route P_1 is 76.9 mm (using Equation (4)). The difference between actual and calculated frequencies is 3.9% due to environmental factors and other radiation losses.

5.3.2. 2nd Harmonic

Patch plane current vectors at the second resonance frequency of 5.026 GHz flow from the patch curve (A_2) sides, over the patch edge, and sink at the feed line/patch interface. Figure 18(b) shows that this line (P_2) generates 5.026 GHz signals. Figure 18(b) shows how long this path is using Equation (5).

$$P_2 = \frac{A_2}{2} + A_3 + P_{l1} + P_{s1} \tag{5}$$

$$f_{r2} = \frac{c}{P_2\sqrt{\varepsilon_{eff}}} \tag{6}$$

The predicted value of the resonance frequency f_{r2} is 5.06 GHz, and the length of the current route P_2 is 29.85 mm (using Equation (6)). Due to environmental factors and other losses, the difference between the observed and predicted frequencies is 0.68 percent.

5.4. Far-Field Pattern

Figures 19(a) and (b) illustrate MC-MSPA with reflector far-field patterns. Simulated and measured far-field radiation patterns at 2.05 GHz and 5.026 GHz match well. The antenna's radiation pattern is bidirectional, symmetrical in both E-planes, and somewhat diminished towards the back. The wide slot monopole antenna construction has some effects. H-planes exhibit omnidirectional radiation at 2.05 GHz. Higher-order modes cause Quasi-Omnidirectional radiation in H-field at 5.026 GHz.

5.5. Gain of the Proposed Antenna

The performances of simulated and measured antenna gains with and without reflector are shown in Figure 20. The antenna's simulated peak gain of 6.47 dBi at 4.6 GHz without a reflector is noticed. The

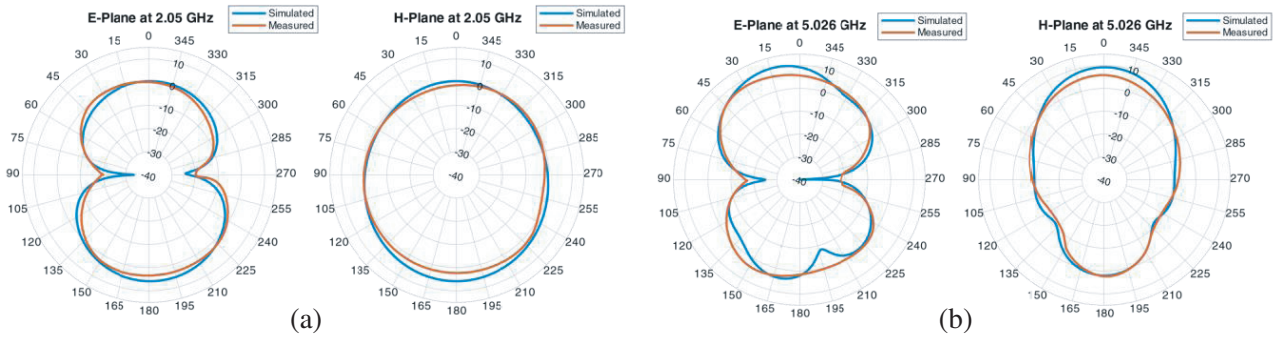

Figure 19. 2D far field radiation pattern E-plane (left) and H-plane (right) at frequencies, (a) 2.05 GHz, (b) 5.026 GHz.

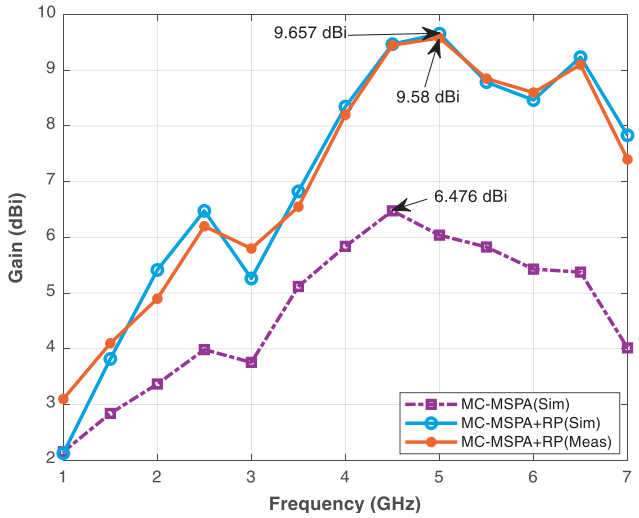

Figure 20. Simulated and measured gains of the antenna with and without reflective plate.

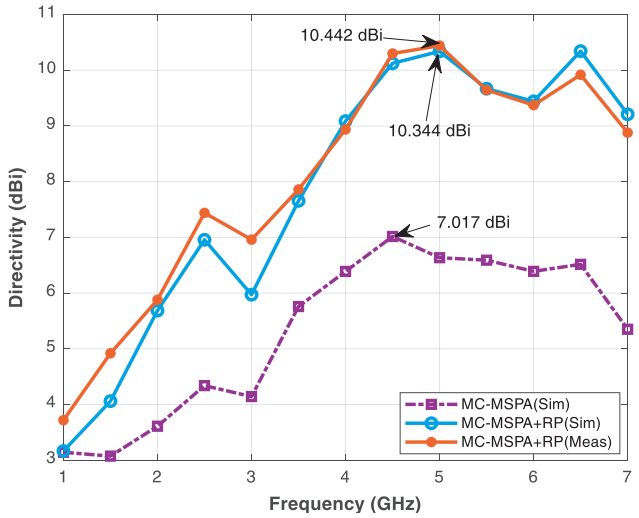

Figure 21. Simulated and measured directivities of the antenna with and without reflective plate.

gain of the antenna with reflector corresponding to frequency response with the interval of 0.5 GHz has been taken, and the maximum peak gain of 9.68 dBi can be observed clearly.

At 5 GHz, the gain was optimized specifically to target Wi-MAX and WLAN applications. A tiny variation between observed and simulated gains may cause measurement losses or antenna construction errors.

5.6. Directivity of the Proposed Antenna

Figure 21 illustrates simulated and measured antenna directivities with and without reflector. The antenna's maximum diversity of 7 dBi at 4.5 GHz has been marked. The antenna's directivity with reflector has a frequency response of 0.5 GHz and a maximum directivity of 10.3 dBi at 5 GHz. Measured and simulated directivities varied somewhat, which may cause losses during measurement or antenna construction errors.

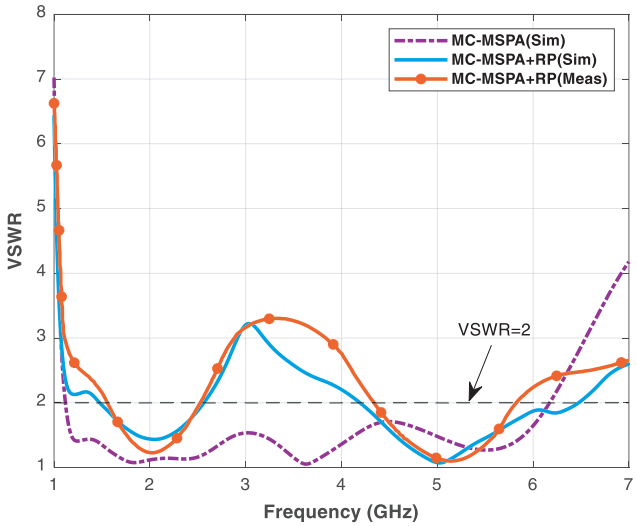

Figure 22. Simulated (a) peak gain and (b) efficiencies of designed antenna.

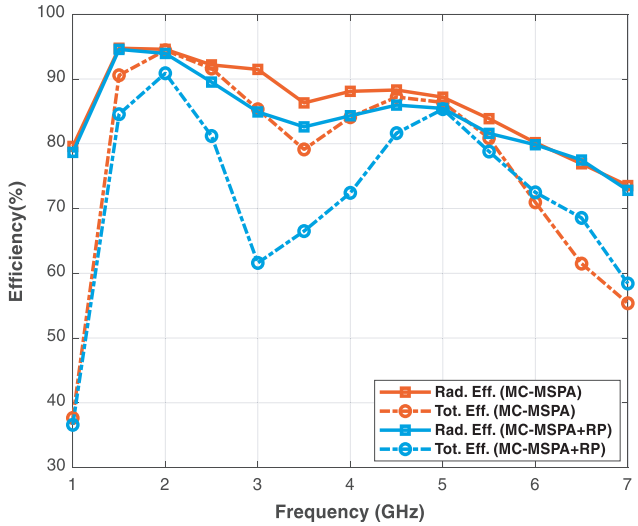

Figure 23. Simulated radiation efficiency and total efficiency of the antenna with and without reflective plate.

Table 3. Percentage change in simulated and measured values.

Parameter	Simulated	Measured	% Change
Resonating Frequency	2.050 GHz	2.073 GHz	1.12
	5.026 GHz	5.173 GHz	2.92
FBW	49.161	42.702	13.14
	40.015	28.864	27.87
IBW	0.996	0.864	13.25
	2.130	1.477	30.66
Max. Gain	9.657	9.58	0.8
Directivity	10.34	10.44	0.97

5.7. Input Impedance and VSWR

The voltage standing wave ratios (VSWRs) of both the designed MC-MSPA and MC-MSPA+RP antennas are given in Figure 22. MC-MSPA reaches large impedance bandwidth, and MC-MSPA+RP antennas reach dual-band output. It can be said that the designed work is good for WLAN and WiMAX uses.

5.8. The Radiation and Total Efficiency of Designed Antenna

Figure 23 illustrates the antenna's radiation efficiency. The antenna sans reflector (MC-MSPA) exhibits 94% total and radiation efficiencies at 2 GHz. At 5 GHz, both antenna efficiencies with reflector loaded (MC-MSPA+RP) are 86% due to the suppression of undesired radiation from reflective plates to improve gain and directivity, especially for Wi-MAX and WLAN applications. Table 3 illustrates MC-MSPA simulation and measurement % variation. Table 4 compares technical structure, dimension, cut-off frequencies, peak gain, and directivity to earlier works.

Table 4. Comparison of various high gain antennas.

Ref.	Technique/ Structure	Dimension Size (λ_g)	F_{low} to F_{High}	Peak Gain/ Directivity
[15]	AMC	$0.69\lambda_g \times 0.53\lambda_g \times 0.15\lambda_g$	2.37–2.47, 3.51–3.67, 5.7–6.01 GHz	8.6 dB
[16]	DGS, Monopole	$0.81\lambda_g \times 0.68\lambda_g \times 0.16\lambda_g$	4.775 to 5.049 GHz	5.49 dB (G) 7.12 dB (D)
[17]	CPW, AMC	$0.49\lambda_g \times 0.43\lambda_g \times 0.04\lambda_g$	2 to 2.6 GHz	6.68 dBi
[18]	Meta surface	$1.46\lambda_g \times 1.46\lambda_g \times 0.12\lambda_g$	2.29 to 2.6 GHz	8.68 dBi
[19]	CPW, FSS	$0.9\lambda_g \times 0.9\lambda_g \times 0.69\lambda_g$	3.05 to 13.4 GHz	5.5–8.5 dBi
[20]	CPW, FSS	$4.17\lambda_g \times 5.31\lambda_g \times 2.65\lambda_g$	3.8 to 10.6 GHz	8 dBi
[21]	CPW, FSS	$3.18\lambda_g \times 3.18\lambda_g \times 0.85\lambda_g$	2.5 to 11 GHz	9 dB
[22]	CPW, FSS	$1.85\lambda_g \times 1.85\lambda_g \times 0.62\lambda_g$	3 to 12 GHz	8.9 dB
[25]	Super-strate	$0.89\lambda_g \times 0.61\lambda_g \times 0.24\lambda_g$	1.79 to 1.83 GHz	8.27 dB
[26]	Z-shaped MTS	$1.5\lambda_g \times 1.5\lambda_g \times 0.51\lambda_g$	4.4 to 7.6 GHz	12.88 dBic
This Work	Wide slot Monopole	$0.87\lambda_g \times 0.87\lambda_g \times 0.24\lambda_g$	1.438 to 2.782 GHz 3.964 to 5.878 GHz	9.65 dBi (G) 10.34 dBi (D)

6. CONCLUSION

The antenna was manufactured on an FR-4 substrate and simulated by CST Studio Suite. In the first step, a mushroom cloud-shaped tuning element is constructed, studied, and experimentally tested in a wide slotted microstrip antenna (MC-MSPA) with a fractional bandwidth of 134.47% from 1.15 GHz to 5.87 GHz for $|S_{11}| < -10$ dB. The antenna has a peak gain of 6.47 dBi at 4.5 GHz, 6.1 at 5 GHz, 7.017 at 4.5 GHz, and -47.37 at 1.88 GHz. In the second step, the high gain mushroom cloud-shaped dual-band microstrip antenna with square reflector plate antenna (MC-MSPA+RP) achieves a peak gain of 9.657 dBi and higher directivity of 10.34 dBi at 5 GHz frequency with dual-band frequency response. A decent response was produced at 17 mm after tweaking the size, spacing of reflective array, and distance

between reflective plate and patch antenna, and 81 mm^2 7×7 square arrays make up the reflecting plate. Dual-band services like Wi-MAX and WLAN can use MC-MSPA+RP's fractional bandwidth of 63% from 1.438 to 2.782 GHz and 38.89% from 3.964 to 5.878 GHz.

REFERENCES

1. Fang, D. G., *Antenna Theory and Microstrip Antennas*, 1st Edition, CRC Press, 2017.
2. Balanis, C. A., *Antenna Theory: Analysis and Design*, 3rd Edition, John Wiley, Hoboken, NJ, 2005.
3. Yang, L., N.-W. Liu, Z.-Y. Zhang, G. Fu, Q.-Q. Liu, and S. Zuo, "A novel single feed omnidirectional circularly polarized antenna with wide AR Bandwidth," *Progress In Electromagnetics Research C*, Vol. 51, 35–43, 2014.
4. Albooyeh, M., N. Kamjani, and M. Shobeyri, "A novel cross-slot geometry to improve impedance bandwidth of microstrip antennas," *Progress In Electromagnetics Research Letters*, Vol. 4, 63–72, 2008.
5. Das, U. and N. Jahan, "Dual band rectangular slotted electromagnetic band gap structure design for improving microstrip patch antenna performance," *2020 11th International Conference on Electrical and Computer Engineering (ICECE)*, 97–100, Dhaka, Bangladesh, Dec. 2020, doi: 10.1109/ICECE51571.2020.9393096.
6. Guo, Q.-Y., Q. W. Lin, and H. Wong, "Directive beam radiation by a fresnel zone plate integrated partially reflective surface for millimeter-wave applications," *2020 14th European Conference on Antennas and Propagation (EuCAP)*, 1–3, Copenhagen, Denmark, Mar. 2020, doi: 10.23919/EuCAP48036.2020.9135424.
7. De Dieu Ntawangaheza, J., L. Sun, Y. Li, and Z. Xie, "Improving bandwidth, gain and aperture efficiency of patch antenna using hybrid AMC ground plane," *Progress In Electromagnetics Research C*, Vol. 103, 71–82, 2020.
8. Huang, J. and V. Jamnejad, "A microstrip array feed for land mobile satellite reflector antennas," *IEEE Trans. Antennas Propagat.*, Vol. 37, No. 2, 153–158, Feb. 1989, doi: 10.1109/8.18701.
9. Qiu, Y., H. Zheng, M. Wang, and E. Li, "Directivity of antenna enhanced by using metasurface structure," *2020 13th UK-Europe-China Workshop on Millimetre-Waves and Terahertz Technologies (UCMMT)*, 1–3, Tianjin, China, Aug. 2020, doi: 10.1109/UCMMT49983.2020.9296050.
10. Joshi, M. P., V. J. Gond, and J. J. Chopade, "Saw-tooth shaped sequentially rotated fractal boundary square microstrip patch antenna for wireless application," *Progress In Electromagnetics Research Letters*, Vol. 94, 109–115, 2020.
11. Hong, T., S.-T. Yu, W. Jiang, and S.-X. Gong, "Gain enhancement of the circularly polarized antenna by fractal technique," *Microw. Opt. Technol. Lett.*, Vol. 55, No. 11, 2656–2659, Nov. 2013, doi: 10.1002/mop.27899.
12. Nurhayati, N., A. Manicoba De-Oliveira, W. Chaihongsa, B. E. Sukoco, and A. K. Saleh, "A comparative study of some novel wideband tulip flower monopole antennas with modified patch and ground plane," *Progress In Electromagnetics Research C*, Vol. 112, 239–250, 2021.
13. Roy, S. and U. Chakraborty, "Gain enhancement of a dualband WLAN microstrip antenna loaded with diagonal pattern metamaterials," *IET Communications*, Vol. 12, No. 12, 1448–1453, Jul. 2018, doi: 10.1049/iet-com.2018.0170.
14. Al-Gburi, A. J. A., I. Ibrahim, M. Y. Zeain, and Z. Zakaria, "Compact size and high gain of CPW-fed UWB strawberry artistic shaped printed monopole antennas using FSS single layer reflector," *IEEE Access*, 1–1, 2020, doi: 10.1109/ACCESS.2020.2995069.
15. Gan, W., X. Lu, J. Yang, Z. Zhang, F. Liu, and S. Yang, "Design of the triple band micro-strip antenna with AMC reflector," *2020 Asia Conference on Computers and Communications (ACCC)*, 7–10, Singapore, Singapore, Sep. 2020, doi: 10.1109/ACCC51160.2020.9347903.

16. Olawoye, T. O. and P. Kumar, "A high gain microstrip patch antenna with slotted ground plane for sub-6 GHz 5G communications," *2020 International Conference on Artificial Intelligence, Big Data, Computing and Data Communication Systems (icABCD)*, 1–6, Durban, South Africa, Aug. 2020, doi: 10.1109/icABCD49160.2020.9183820.
17. Yuan, Y.-N., J.-J. Feng, and X.-L. Xi, "Design of wearable antenna with compact artificial magnetic conductor reflecting plate," *2017 Sixth Asia-Pacific Conference on Antennas and Propagation (APCAP)*, 1–3, Xi'an, Oct. 2017, doi: 10.1109/APCAP.2017.8420366.
18. Chung, K. L. and S. Chaimool, "Broadside gain and bandwidth enhancement of microstrip patch antenna using a MNZ-metasurface," *Microw. Opt. Technol. Lett.*, Vol. 54, No. 2, 529–532, Feb. 2012, doi: 10.1002/mop.26574.
19. Kundu, S., A. Chatterjee, S. K. Jana, and S. K. Parui, "A compact umbrella-shaped UWB antenna with gain augmentation using frequency selective surface," *Radioengineering*, Vol. 27, No. 2, 448–454, Jun. 2018, doi: 10.13164/re.2018.0448.
20. Abdulhasan, R. A., R. Alias, K. N. Ramli, F. C. Seman, and R. A. AbdAlhameed, "High gain CPW-fed UWB planar monopole antennabased compact uniplanar frequency selective surface for microwave imaging," *Int. J. RF Microw. Comput. Aided Eng.*, Vol. 29, No. 8, Aug. 2019, doi: 10.1002/mmce.21757.
21. Yuan, Y., X. Xi, and Y. Zhao, "Compact UWB FSS reflector for antenna gain enhancement," *IET Microwaves, Antennas & Propagation*, Vol. 13, No. 10, 1749–1755, Aug. 2019, doi: 10.1049/iet-map.2019.0083.
22. Tahir, F. A., T. Arshad, S. Ullah, and J. A. Flint, "A novel FSS for gain enhancement of printed antennas in UWB frequency spectrum," *Microw. Opt. Technol. Lett.*, Vol. 59, No. 10, 2698–2704, Oct. 2017, doi: 10.1002/mop.30789.
23. Madhav, B. T. P., A. V. Chaitanya, R. Jayaprada, and M. Pavani, "Circular monopole slotted antenna with FSS for high gain applications," *ARPN Journal of Engineering and Applied Sciences*, Vol. 11, No. 15, 7, 2016.
24. Ge, Y., K. P. Esselle, and T. S. Bird, "The use of simple thin partially reflective surfaces with positive reflection phase gradients to design wideband, low-profile EBG resonator antennas," *IEEE Trans. Antennas Propagat.*, Vol. 60, No. 2, 743–750, Feb. 2012, doi: 10.1109/TAP.2011.2173113.
25. Tian, H., J. Wang, D. Han, and X. Wang, "A gain-enhanced dual-band microstrip antenna using metasurface as superstrate configuration," *ACES Journal*, Mar. 2022, doi: 10.13052/2021.ACES.J.361210.
26. Supreeyatitikul, N., A. Boonpoonga, and C. Phongcharoenpanich, "Z-shaped metasurface-based wideband circularly polarized Fabry-Pérot Antenna for C-band satellite technology," *IEEE Access*, Vol. 10, 59428–59441, 2022, doi: 10.1109/ACCESS.2022.3179360.